The Japanese Geotechnical Society

Soils and Foundations

SOILS
AND
FOUNDATIONS

Strain localization characteristics of loose saturated Toyoura sand in undrained cyclic torsional shear tests with initial static shear

Gabriele Chiaro[a,1], Takashi Kiyota[b], Junichi Koseki[b,*]

[a]*Centre for Geomechanics and Railway Engineering, University of Wollongong, Australia*
[b]*Institute of Industrial Science, University of Tokyo, Japan*

Abstract

Strain localization, or the formation of shear bands, is a key aspect in understanding soil failure mechanisms. While efforts have been made in terms of measuring the shear band properties and the stress–strain behavior within shear bands, there are still uncertainties regarding when shear bands initiate and their influence on the development of large ground deformation. In this paper, the limiting value of shear strain, at which strain localization appears during undrained cyclic torsional shear tests with initial static shear, performed on loose Toyoura sand specimens ($Dr=44$–48%) up to a single amplitude of shear strain exceeding 50%, was evaluated. Non-uniform specimen deformation was observed at strain levels larger than 20%. However, the onset of strain localization could not be defined on the basis of visual observations. Therefore, the limiting values for half of the double amplitude ($\gamma_{DA}/2$) and single amplitude (γ_{SA}) shear strain, to initiate strain localization, were determined from test results based on changes in the deviator stress response and strain accumulation properties as well as changes in the strain-softening behavior during cyclic shear. It was found that γ_{SA} is a more appropriate parameter than $\gamma_{DA}/2$. Irrespective of the static shear stress level, the limiting strain value for γ_{SA} was evaluated to be in the range of 23–28% for liquefied loose Toyoura sand specimens (i.e., stress reversal and intermediate tests). Alternatively, the limiting strain value could not be properly defined when liquefaction did not occur (i.e., non-reversal stress tests), although various methods were employed.

*Corresponding author. Tel.: +82 31 290 7224; fax: +82 31 299 4134.
E-mail addresses: gchiaro@uow.edu.au (G. Chiaro),
kiyota@iis.u-tokyo.ac.jp (T. Kiyota),
koseki@iis.u-tokyo.ac.jp (J. Koseki).
[1]Formerly at Department of Civil Engineering, University of Tokyo, Japan.

ELSEVIER **Production and hosting by Elsevier**

1. Introduction

The failure of cohesionless materials, such as sand, is typically the result of strain localization, i.e., the concentration of shear deformation in a narrow zone of intense shearing commonly referred to as a shear band. In general, the shear banding process begins at the state when the mobilized strength of the geomaterials reaches its peak and develops as shear deformation continues. A proper understanding of the strain localization mechanisms (formation and evolution) is vital to most geotechnical problems, including slope stability and soil liquefaction.

Since the late 1950s, much effort has been made in the measurement of shear band properties (thickness and orientation, etc.) and the stress–strain behavior within shear bands. Researchers have found that strain localization is affected by various factors, such as the mean diameter of the particles, the confining stress, the density, the shear conditions, etc. In triaxial tests, a single well-defined shear band rarely develops (Lade, 1982; Alshibli et al., 2003). Instead, a complex internal failure pattern involving the formation of multiple shear bands may be observed using advanced visualization techniques, e.g. a laser technique (Tatsuoka et al., 1990), computed tomography (Desrues et al., 1996), stereophotography (Finno et al., 1996), an image analysis (Jang and Frost, 2000), etc. Due to the simplicity of observation and data analyzing, a number of studies on strain localization in sand have been conducted using plane strain compression tests with transparent confining plates (Finno et al., 1997; Alshibli and Sture, 2000; Viggiani et al., 2001 among others). Above all, the results indicate that the failure of plane strain specimens always occurs along a well-defined shear plane (Peters et al., 1988). Similar to plane strain tests, well-defined shear bands are also seen to develop in ring shear tests (e.g., Sadrekarimi and Olson, 2009, 2010), but they do not develop freely at any orientation apart from the horizontal one. Alternatively, a torsional shear apparatus is capable of simulating the rotation in the major principal stress direction during the loading process and shearing can be examined at very large displacements (Kiyota et al., 2008). However, shear banding observation in torsional shear tests may complicate the analysis process due to the surface of cylindrical specimens (Wahyudi et al., 2012). Although considerable information has been provided by these tests, there are still uncertainties regarding when shear bands initiate and their influence on large ground deformation development, especially in the case of loose (contractive) sand subjected to cyclic undrained shear loading (i.e., liquefiable soils). This topic is investigated in the present paper.

Experience from past large-magnitude earthquakes (e.g., 1964 Great Alaskan, USA; 1964 Niigata, Japan; 1983 Nihonkai–Chubu, Japan; 1995 Hyogoken–Nambu or Kobe, Japan; etc.) indicates that extremely large horizontal ground deformation can occur in liquefied sandy deposits in coastal or river areas. When the lateral spreading of liquefied deposits takes place, the ground displacement may exceed several meters, even in very gentle slopes (e.g., Hamada et al., 1994) or in level ground behind retaining walls (e.g., Ishihara et al., 1996), resulting in severe damage to buildings, infrastructures and lifeline facilities. In order to thoroughly investigate the above liquefaction-induced large strain, Kiyota et al. (2008) modified a torsional shear apparatus for enlarging the range of torsional displacement, and performed a series of undrained cyclic torsional shear tests up to a double amplitude shear strain (γ_{DA}) of about 100% on Toyoura sand specimens isotropically consolidated at different density states. They reported that there is a limiting value of γ_{DA} to initiate strain localization, which increases with a decrease in the relative density of the specimen. Later, Kiyota et al. (2010) found the limiting values to initiate strain localization observed in torsional shear tests to be consistent with the maximum amounts of liquefied-induced ground displacement observed in previous shaking table model tests (e.g., Yasuda et al., 1992) and most of the relevant case studies (e.g., Hamada et al., 1988). These features are reasonable considering the reduction in mobilized cyclic shear stress in liquefied soils due to the degradation of shear resistance. As long as the liquefied soil layer remains in uniform deformation, such limiting values, which may depend on the soil type and the density among others, may be used to estimate the maximum amount of ground displacement due to liquefaction in sandy deposits (Kiyota et al., 2010). In the tests presented by Kiyota et al. (2008), however, the presence of the initial static shear (i.e., sloped ground conditions) was not taken into consideration.

Chiaro et al. (2012) investigated the role which static shear plays in the large deformation behavior of saturated sand during undrained cyclic shear loading by performing a series of undrained cyclic torsional shear tests on loose saturated Toyoura sand specimens up to the single amplitude shear strain (γ_{SA}) of about 50%. Based on changes in the deviator stress response and strain accumulation properties, as well as changes in the strain-softening behavior during cyclic shear, the test results presented by Chiaro et al. (2012) were analyzed in this paper in order to evaluate the possible correlation between the extent of the initial static shear and the limiting value for γ_{SA} or γ_{DA} required to initiate strain localization.

2. Sand specimen deformation in cyclic torsional shear tests with initial static shear

Loose Toyoura sand specimens, ($e=0.819$–0.833 corresponding to $Dr=44$–48%) having the dimensions of 150 mm in outer diameter, 90 mm in inner diameter and 300 mm in height, were prepared by the air pluviation method and then saturated. The specimens were isotropically consolidated to an effective mean stress of $p_0'=100$ kPa with a back pressure of 200 kPa, and then monotonically sheared while maintaining drained conditions, in order to apply a specific value of initial static shear representative of sloping ground conditions. Finally, to study the behavior of sand under seismic conditions (liquefaction resistance and/or the development of large deformation), undrained torsional shear loading was applied at a constant shear strain rate (2.5%/min). As listed in Table 1, cyclic loading tests were performed over a wide range of initial static shear (τ_{static}) from 0 to 25 kPa. Two levels of cyclic shear stress amplitude (τ_{cyclic}), 16 and 20 kPa, were employed in order to consider various combinations of initial static and cyclic shear stress. It should be noted that during the process of undrained cyclic torsional loading, the vertical displacement of the top cap was prevented for the purpose of simulating, as much as possible, the simple shear condition that the ground undergoes during horizontal seismic excitation. Three

Table 1
Undrained cyclic torsional shear tests performed by Chiaro et al. (2012).

Test	e	Dr	τ_{cyclic}	τ_{static}	τ_{max}	τ_{min}	R	Loading pattern
1	0.825	46.4	16	0	+16	−16	1.00	Reversal
2	0.828	45.5	16	5	+21	−11	0.52	Reversal
3	0.824	46.6	16	10	+26	−6	0.23	Reversal
4	0.833	44.2	16	15	+31	−1	0.03	Reversal
5	0.825	46.5	16	16	+32	0	0.00	Intermediate
6	0.820	47.9	16	17	+33	+1	−0.03	Non-reversal
7	0.829	45.3	16	20	+36	+4	−0.11	Non-reversal
8	0.819	48.1	20	0	+20	−20	1.00	Reversal
9	0.819	48.0	20	5	+25	−15	0.60	Reversal
10	0.828	45.6	20	10	+30	−10	0.33	Reversal
11	0.832	44.4	20	15	+35	−5	0.14	Reversal
12	0.823	46.9	20	20	+40	0	0.00	Intermediate
13	0.826	46.1	20	25	+45	+5	−0.11	Non-reversal

e : void ratio, Dr : relative density (%) measured at an isotropic stress state of $\sigma'_c = 100$ kPa.
τ_{cyclic} : cyclic shear stress (kPa), τ_{static} : initial static shear stress (kPa).
$\tau_{max} = \tau_{static} + \tau_{cyclic}$: maximum combined shear stress (kPa).
$\tau_{min} = \tau_{static} - \tau_{cyclic}$: minimum combined shear stress (kPa).
$R = -(\tau_{min}/\tau_{max})$: degree of reversal loading (Yoshimi and Oh-oka, 1975).
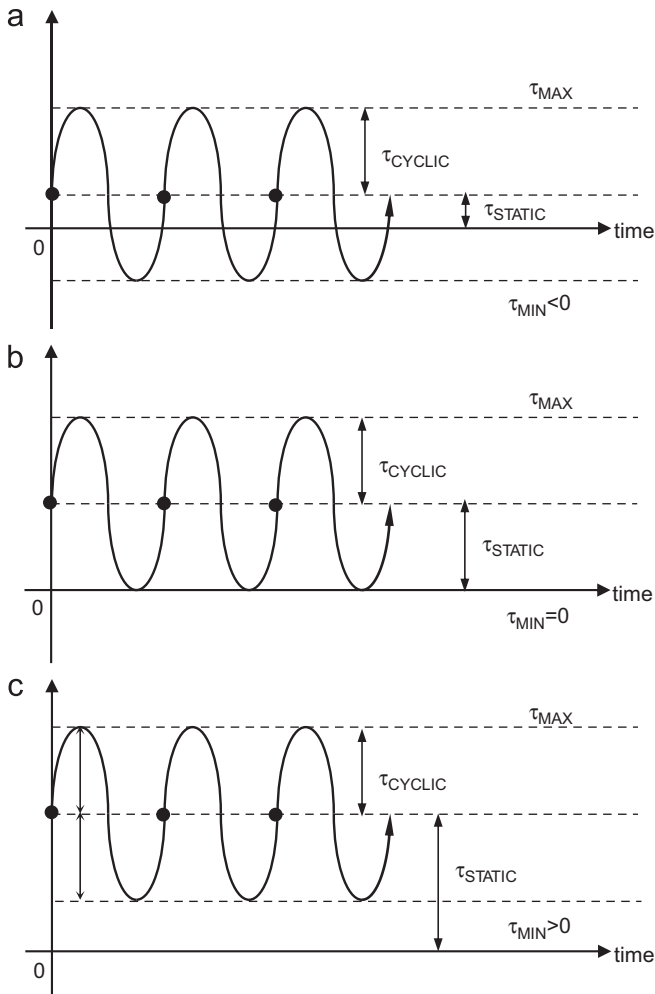

Fig. 1. Scheme of cyclic torsional shear loading (after Chiaro et al., 2012):(a) stress reversal, (b) intermediate and (c) non-reversal.
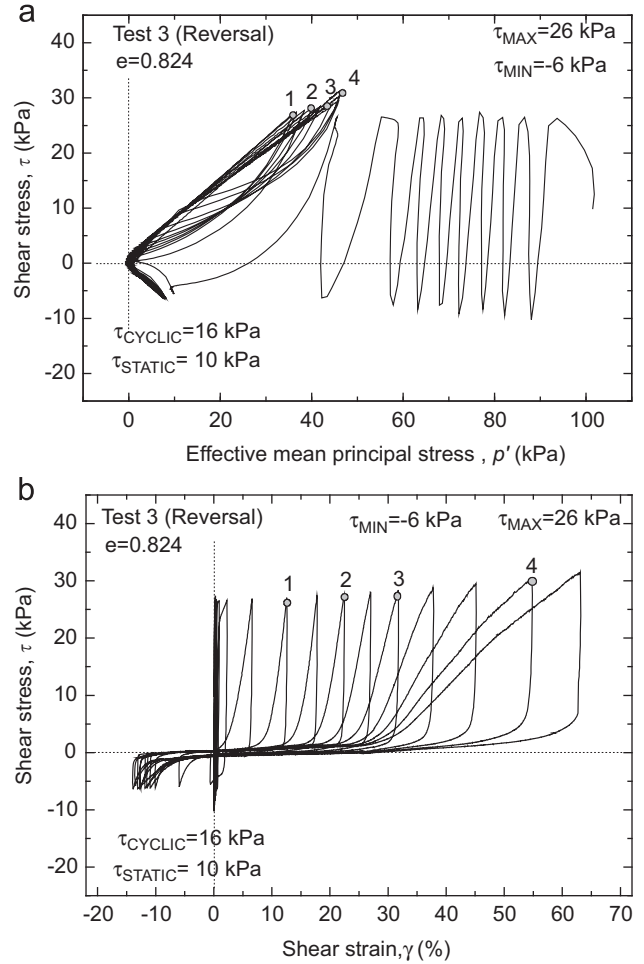

Fig. 2. Typical test results employing stress reversal loading pattern: (a) effective stress path and (b) stress–strain relationship.

types of cyclic loading patterns were employed, namely, stress reversal, intermediate and non-reversal, as schematically shown in Fig. 1. Readers may refer to Chiaro et al. (2012) for details on the torsional shear apparatus, test procedure and material properties.

Typical test results are presented in Figs. 2–4, in terms of the effective stress paths and the stress–strain relationships. The corresponding specimen deformation at several states, numbered 1 through 4 in Figs. 2–4, are shown in Photos 1–3, respectively.

As shown in Fig. 2, in the case of the reversal loading pattern (e.g., Test 3 in Table 1), cyclic mobility was observed in the effective stress path, where the effective stress recovered repeatedly after reaching the state of zero effective stress (i.e., full liquefaction). It was accompanied by a significant development of shear strain as evidenced by the stress–strain relationship. Photo 1 shows the specimen deformation observed for this test. At State 1 ($\gamma = 12\%$), the deformation was almost uniform, except for the regions close to the pedestal and the top cap that are affected by the end restraint; the outer membrane appeared slightly wrinkled. At State 2 ($\gamma = 22\%$), the outer membrane was visibly wrinkled and the deformation of the
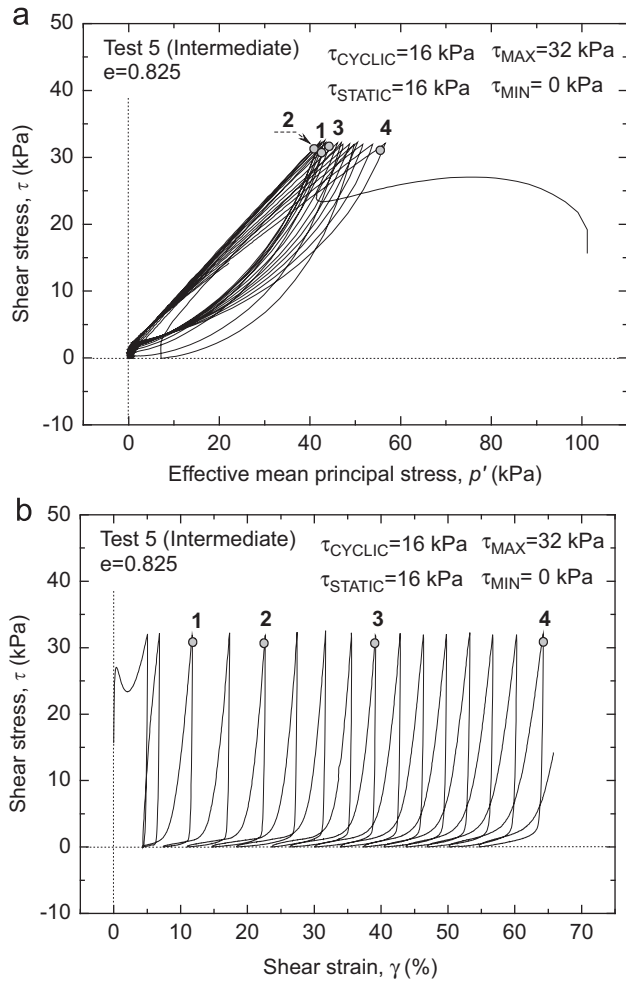
Fig. 3. Typical test results employing intermediate loading pattern: (a) effective stress path and (b) stress–strain relationship.

Fig. 4. Typical test results employing non-reversal loading pattern: (a) effective stress path and (b) stress–strain relationship.

specimen started to localize in the region near the top cap probably due to the formation of water film (Kokusho, 1999, 2000). At State 3 ($\gamma = 31\%$), the localization of the specimen deformation developed clearly in the upper part of the specimen. On the other hand, in the bottom part, the uniformity of the specimen deformation could be maintained even though many wrinkles appeared. At State 4 ($\gamma = 54\%$), the specimen was almost twisted near the top cap.

Fig. 3 shows the case of the intermediate loading pattern (e.g., Test 5). This type of test shows behavior that is similar to the behavior of the reversal case. In other words, after reaching a fully liquefied state, progressive large deformation develops while showing cyclic mobility. However, the intermediate loading pattern can be distinguished from the reversal loading pattern by looking at the specimen deformation shown in Photo 2. At State 1 ($\gamma = 11\%$), the deformation was almost uniform, except for the regions close to the pedestal and the top cap that are affected by the end restraint. At State 2 ($\gamma = 23\%$), the outer membrane was extensively wrinkled. Nevertheless, it should be noted that the type of wrinkles observed in this test have a different meaning than those observed in the reversal test.
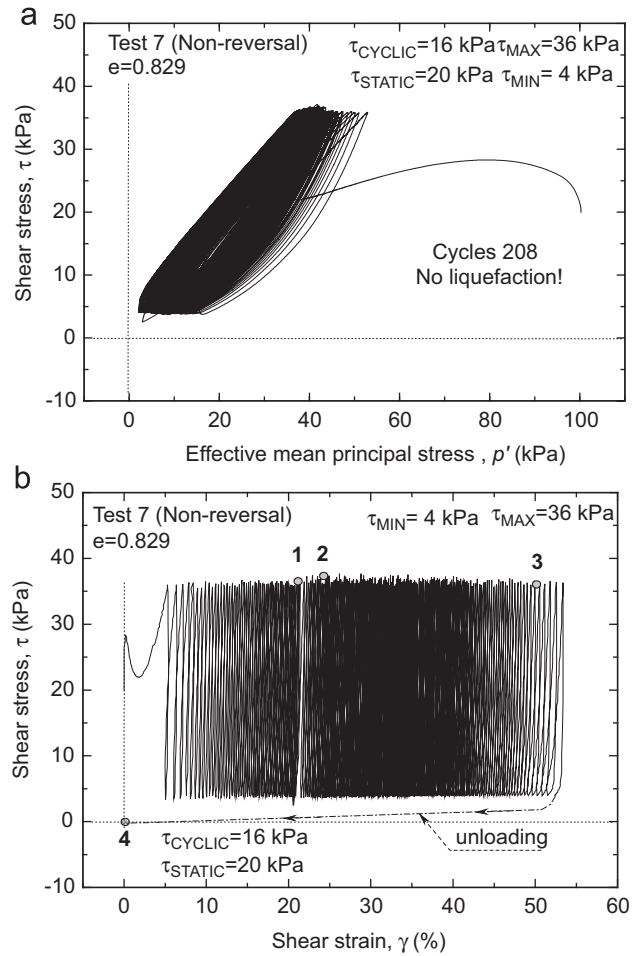
In fact, in this test, the specimen deformation pattern shifts when it intersects a wrinkle (see the comparison of the deformation pattern within the red circles in Photos 1 and 2(b)). In addition, the lateral surface of the specimen was no more smooth, as can be seen in Photo 2(b). This behavior suggests that the formation of several shear bands took place and that several parts of the specimen moved due to the different extents of the deformation. At State 3 ($\gamma = 39\%$), the diameter of the specimen decreased at several locations, as marked by the arrows, possibly due to the formation of shear bands. Finally, at State 4 ($\gamma = 64\%$), the specimen was completely twisted.

Fig. 4 illustrates the case of the non-reversal loading pattern (e.g., Test 7). The state of zero effective stress was not achieved even after applying 208 loading cycles. However, a large shear strain exceeding 50% was reached, and the formation of a single spiral shear band could be observed. Specimen deformation observed for this test is shown in Photo 3. At State 1 ($\gamma = 21\%$), the deformation was rather uniform except for the regions close to the pedestal and the top cap that are affected by the end restraint. At State 2 ($\gamma = 25\%$), the outer membrane was wrinkled at several locations due to local water drainage.
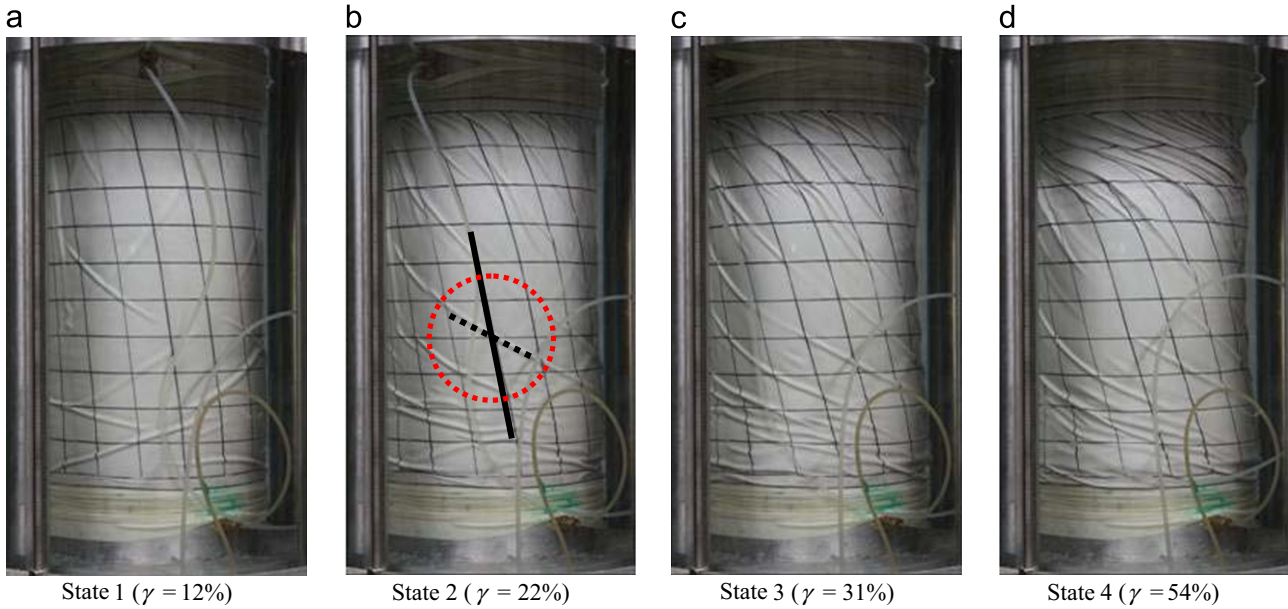
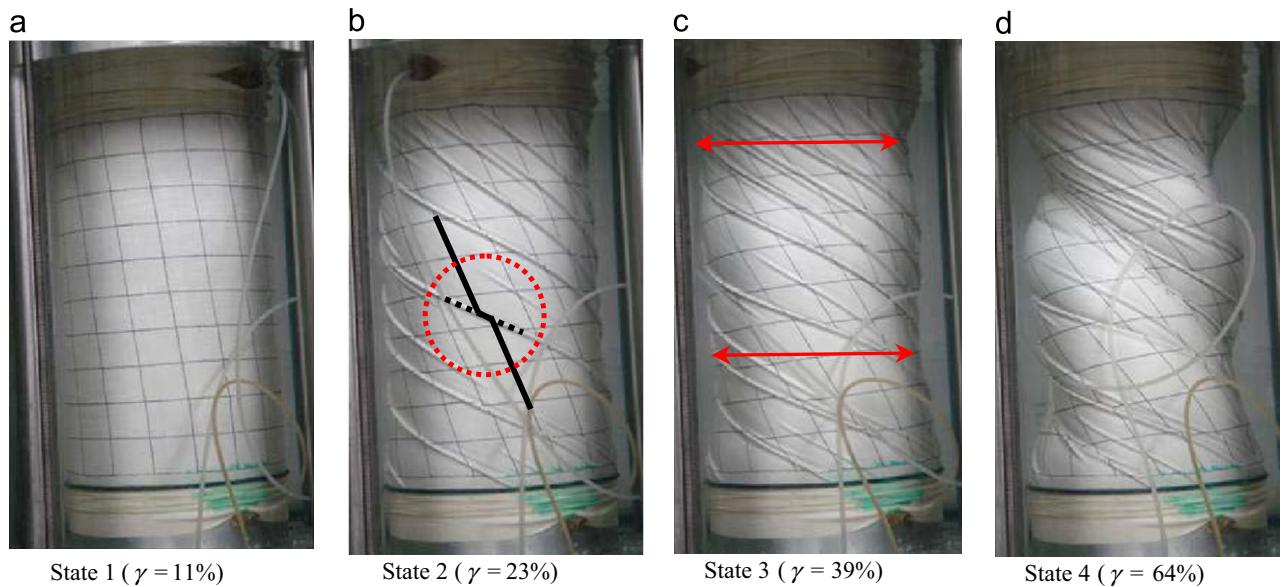Photo 1. Specimen deformation at States 1 through 4 shown in Fig. 2.

State 1 ($\gamma = 12\%$)   State 2 ($\gamma = 22\%$)   State 3 ($\gamma = 31\%$)   State 4 ($\gamma = 54\%$)

Photo 2. Specimen deformation at States 1 through 4 shown in Fig. 3.

State 1 ($\gamma = 11\%$)   State 2 ($\gamma = 23\%$)   State 3 ($\gamma = 39\%$)   State 4 ($\gamma = 64\%$)

At State 3 ($\gamma = 50\%$), the outer membrane was extensively wrinkled from the bottom to the top. At State 4 ($\gamma = 0\%$, after unloading to $\tau = 0$ while keeping undrained condition), the formation of a single spiral shear band could be observed (as marked by the dotted lines).

3. Strain localization during cyclic loading

In this section, the effect of the initial static shear stress on the limiting value of the shear strain at which strain localization appears during undrained cyclic torsional shear tests was evaluated based on changes in the deviator stress response and strain accumulation properties as well as changes in strain-softening during cyclic shear.

3.1. Evaluation of strain localization based on changes in deviator stress response and strain accumulation properties

Tatsuoka et al. (1986) performed drained monotonic torsional shear tests on hollow cylindrical Toyoura sand specimens with a void ratio in the range of 0.665–0.808, while keeping the vertical (σ_v') and horizontal (σ_h') effective stress values constant. They reported that vertical strain accumulated on the extension side due to the mobilization of positive dilatancy, and that it decreased suddenly when a shear band formed in the specimen.

Kiyota et al. (2008) found that changes in the deviator stress q ($= \sigma_v' - \sigma_h'$) response observed in undrained torsional shear tests, in which any vertical displacement
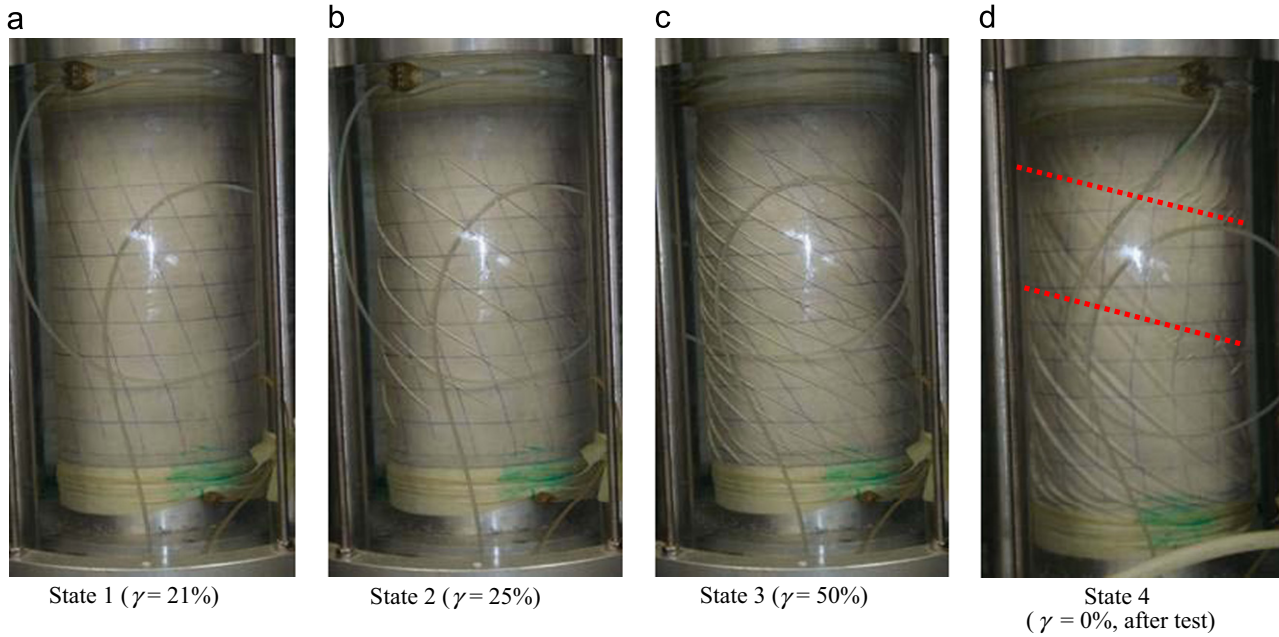
Photo 3. Specimen deformation at States 1 through 4 shown in Fig. 4.

of the top cap was prevented (i.e., simple shear conditions), to be consistent with the behavior observed during drained monotonic torsional shear tests by Tatsuoka et al. (1986). Therefore, they considered the state at which the amplitude of deviator stress decreases as the limiting state to initiate the formation of shear bands, and thus, strain localization. Furthermore, it was found to be accompanied by an increase in the single amplitude shear strain increment ($\Delta\gamma_{SA}$). As a result, these features imply that the stress–strain characteristics of the specimen were changed by the formation of shear bands and the initiation of strain localization in the specimen.

In this study, non-uniform specimen deformation was observed at strain levels higher than 20%. However, similar to Kiyota et al. (2008), the initiation of strain localization could not be clearly defined on the basis of visual observations. Hence, to address this issue and to evaluate the effects of the initial static shear on the specimen deformation behavior, the attempt made by Kiyota et al. (2008) was employed. Consequently, from the analysis of deviator stress responses (Fig. 5) and stress–strain relationships (Fig. 6), the following two states were defined: i) State A: the state at which the q value suddenly decreases and ii) State B: the state at which changes in the strain accumulation properties (i.e., rises in the single amplitude shear strain increment, $\Delta\gamma_{SA}$) were observed. It should be noted that the deviator stress was corrected for the effects of membrane force, which is discussed in the Appendix A.

The values for shear strain at State A and State B were measured in terms of $\gamma_{DA}/2$, as employed by Kiyota et al. (2008), and γ_{SA}, which is usually used to describe the effects of static shear on the deformation behavior (Chiaro et al., 2012). Definitions of γ_{DA} and γ_{SA} are given in Fig. 7. Note that these

shear strain levels are the strain levels which developed during undrained cyclic loading; they do not account for the initial shear strain (γ_{static}) induced by drained shear loading before the undrained one. Nevertheless, under the test conditions employed in this study, the correction for such γ_{static} could be disregarded since it was less than 0.24%, as evaluated by Chiaro (2010) and reported here in Table 2.

To consider the effects of the initial static shear stress and its combination with cyclic shear stress, the shear strain was plotted in Figs. 8 and 9 against the degree of reversal loading (R), which can be calculated by Eq. (1) as proposed by Yoshimi and Oh-oka (1975):

$$R = \frac{\tau_{cyclic} - \tau_{static}}{\tau_{cyclic} + \tau_{static}} = -\frac{\tau_{min}}{\tau_{max}} \tag{1}$$

where τ_{cyclic} is the single amplitude cyclic shear stress, τ_{static} is the initial static shear stress and τ_{max} ($= \tau_{static} + \tau_{cyclic}$) and τ_{min} ($= \tau_{static} - \tau_{cyclic}$) are, respectively, the maximum and the minimum values of shear stress applied during cyclic loading (Chiaro et al., 2012).

In Figs. 8 and 9, it can be seen that the lower the R value the lower the $\gamma_{DA}/2$ value. Such a reduction in $\gamma_{DA}/2$ is due to the fact that by applying initial static shear, the stress condition becomes non-symmetric with respect to the initial stress state (see Fig. 7). In addition, a sudden drop in the value of $\gamma_{DA}/2$ was observed in the case of the intermediate and the non-reversal loading tests. Alternatively, the γ_{SA} value is rather constant (i.e., independent of static shear) in the case of the reversal loading tests, and then suddenly increases in the case of the intermediate and the non-reversal loading tests.

Based on these considerations, for specimens showing liquefaction (i.e., stress reversal tests), γ_{SA} appears to be a more appropriate parameter than $\gamma_{DA}/2$ for evaluating the
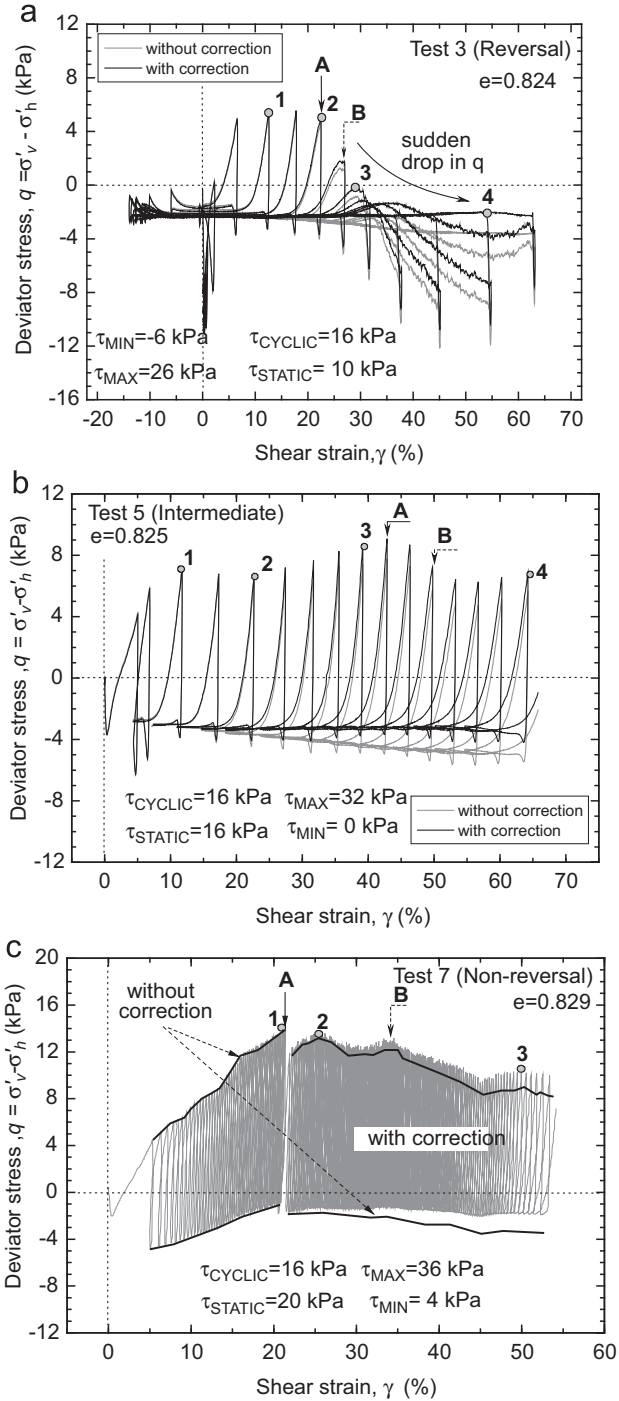
Fig. 5. Changes in deviator stress response with/without correction for membrane force: (a) stress reversal (c.f. Fig. 2), (b) intermediate (c.f. Fig. 3) and (c) non-reversal (c.f. Fig. 4).
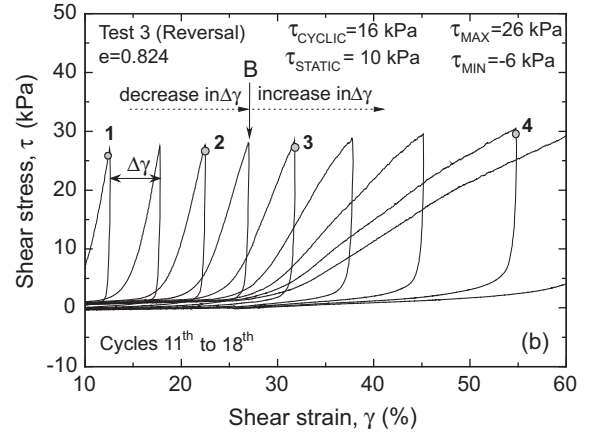

Fig. 6. Typical changes in shear strain accumulation properties during cyclic loading based on stress–strain relationship (c.f. Fig. 4).
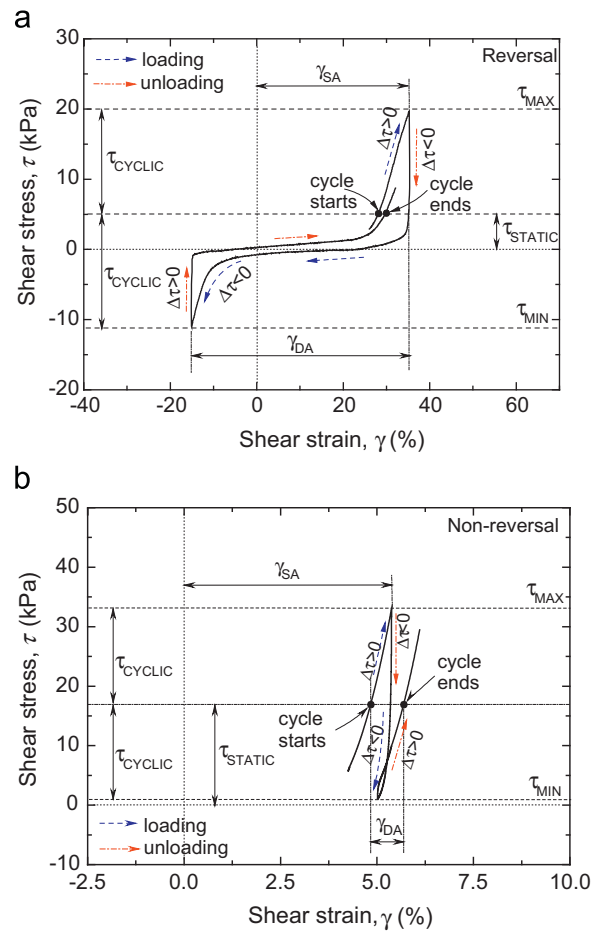

Fig. 7. Definition of double amplitude shear strain (γ_{DA}) and single amplitude shear strain (γ_{SA}) used in this study for: (a) reversal loading pattern and (b) non-reversal loading pattern.

strain localization value. Hence, based on the test results in Figs. 8 and 9(b), it was defined as:

(i) $\gamma_{SA,avg}^{A} \cong 23\%$, which represents the average strain value at which q suddenly decreases (State A), i.e., changes in deviator stress

(ii) $\gamma_{SA,avg}^{B} \cong 28\%$, which corresponds to the average strain value at which changes in strain accumulation take place (State B).

Note that in Fig. 5(c), a sudden drop in q can be observed, which may be evidence of the formation of a shear band within the specimen. However, as illustrated in Photo 3, from the pictures that were taken before (State 1,

Table 2
Value of static shear strain (γ_{static}) obtained by monotonic drained torsional shear tests on loose Toyoura sand specimen ($e=0.811$), (Chiaro, 2010).

τ_{static} (kPa)	γ_{static} (%)	τ_{static} (kPa)	γ_{static} (%)
5	0.02	40	0.98
10	0.03	50	2.11
15	0.09	60	3.86
20	0.16	70	6.79
25	0.24	77.6[*]	10.7[*]
30	0.38		

[*]Shear stress and shear strain at peak state.
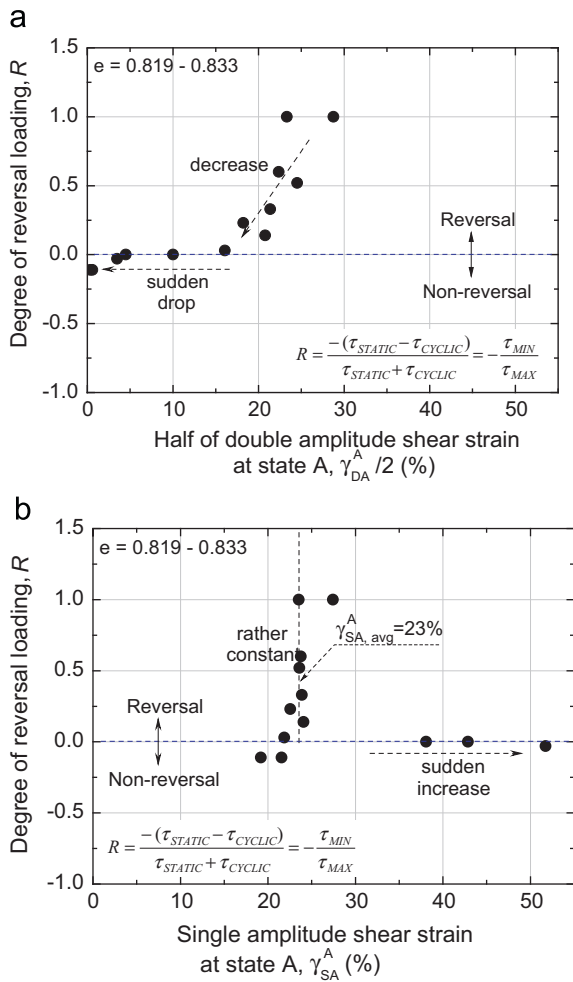
Fig. 8. Changes in deviator stress response (State A) evaluated in terms of: (a) half of double amplitude shear strain and (b) single amplitude shear strain.
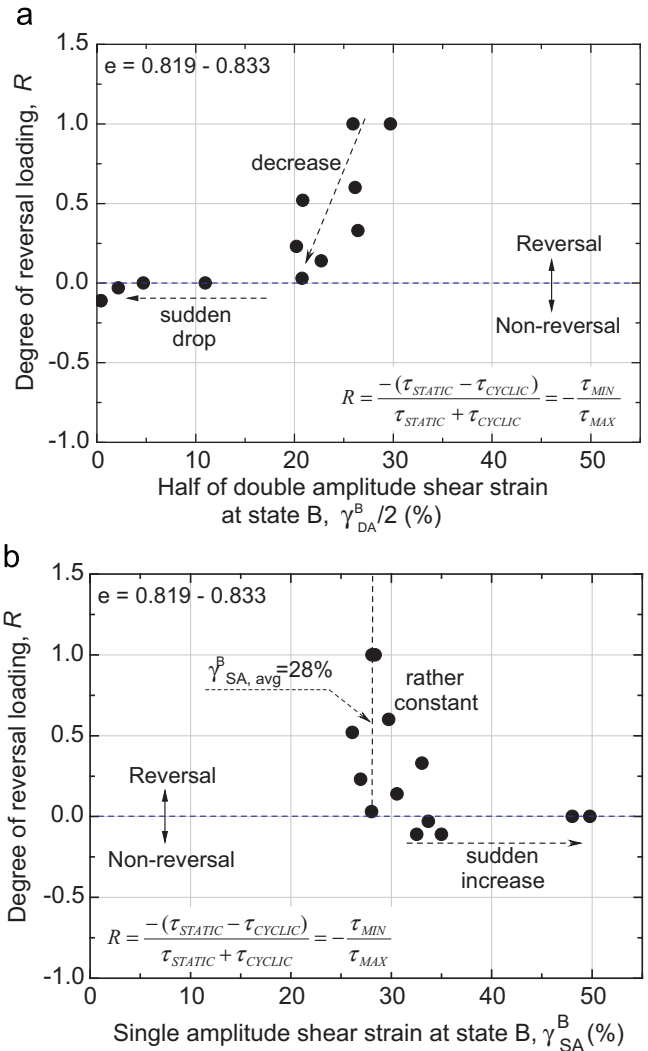

Fig. 9. Changes in shear strain behavior (State B) evaluated in terms of: (a) half of double amplitude shear strain and (b) single amplitude shear strain.

at shear strain levels of about 20–30%. This suggests that an evaluation of the strain localization based on changes in the deviator stress response and strain accumulation properties may be inappropriate for both intermediate and non-reversal stress loading tests.

3.2. Evaluation of strain localization based on changes in strain-softening behavior at large shear strain levels

In order to confirm the validity of the methods employed in the previous section to define the limiting value of γ_{SA} to initiate strain localization (i.e., the formation of shear bands) of the specimens, the strain-softening behavior (i.e., the reduction in shear strength) of sand during cyclic loading was investigated. For this purpose, the shear stress ratio defined using the modified shear stress and the modified current effective mean principal stress, $(\tau - \Delta\tau)/(p' + \Delta p')$, as originally introduced by Koseki et al. (2005), was employed.

$\gamma=21\%$) and after (State 2, $\gamma=25\%$) this change in the q response, no clear shear band can be seen.

As shown in Figs. 8 and 9(b), in the case of the intermediate and the non-reversal loading tests, the limiting values for γ_{SA}, evaluated on the basis of changes in either the deviator stress response or the strain accumulation properties, increase drastically up to about 50%, while the visual observations show that the non-uniform deformation of specimens appears

Koseki et al. (2005) carried out a series of undrained cyclic torsional shear tests in order to investigate the liquefaction properties of Toyoura sand under low confining stress. The test results revealed that the effective stress path did not pass through the origin ($\tau = p' = 0$). They reported that this behavior is possibly affected by the following factors: (i) the effect of interlocking among sand particles that could be mobilized even under zero effective stress states, (ii) errors in measured deviator stress q, which could cause apparent non-zero values of p' and (iii) the viscous interaction between pore water and the surface of sand grains, as pointed out by Towhata and Gallage (1993) among others. Therefore, in the attempts made by Koseki et al. (2005), apparent changes in the effective mean principal stress state ($\Delta p'$) and the shift in shear stress ($\Delta \tau$) were introduced to correct the effects of the mobilization of shear resistance under extremely low effective stress states.

$\Delta \tau$ and $\Delta p'$ are very sensitive parameters and their calibration is not an easy task. Koseki et al. (2005) and Kiyota et al. (2008) attempted to use constant values for $\Delta \tau$ and $\Delta p'$. However, in Chiaro (2010), it was found that this approach is not suitable for describing the strain-softening behavior of sand with initial static shear. In fact, the values for $\Delta \tau$ and $\Delta p'$ may change significantly with the cycle number. Thus, in this study, an attempt was made to use the current values for $\Delta \tau$ and $\Delta p'$ to properly correct the stress–strain relationship for the effects of interlocking among sand grains in undrained torsional shear tests with initial static shear.

Fig. 10 shows a typical close-up around the origin of the effective stress path and an evaluation of $\Delta \tau$ and $\Delta p'$. In Fig. 11, the values for $\Delta \tau$ and $\Delta p'$ measured at each cycle of loading for Test 8 are presented. It should be noted that in the case of reversal stress loading, the values for $\Delta \tau$ and $\Delta p'$ can be evaluated only after the stress state has entered the post-liquefaction state (i.e., cyclic mobility state). Therefore, in the pre-liquefaction state, the values for $\Delta \tau$ and $\Delta p'$ are taken as zero (i.e., $\Delta \tau = \Delta p' = 0$). It
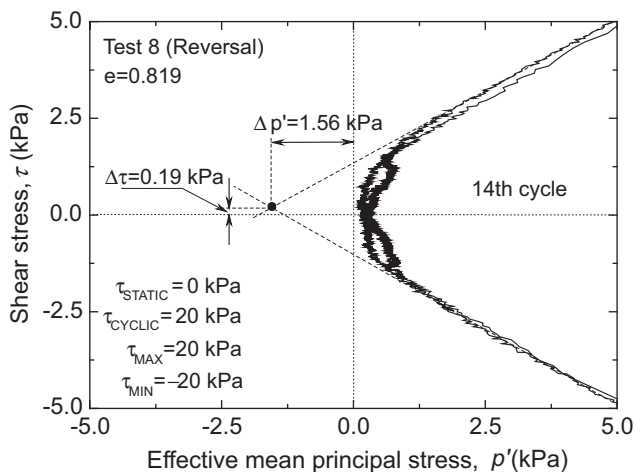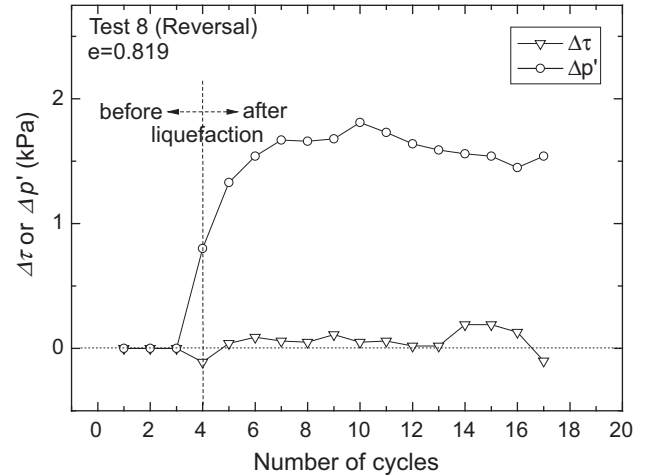

Fig. 11. Typical values for $\Delta \tau$ and $\Delta p'$ measured at each cycle of loading.
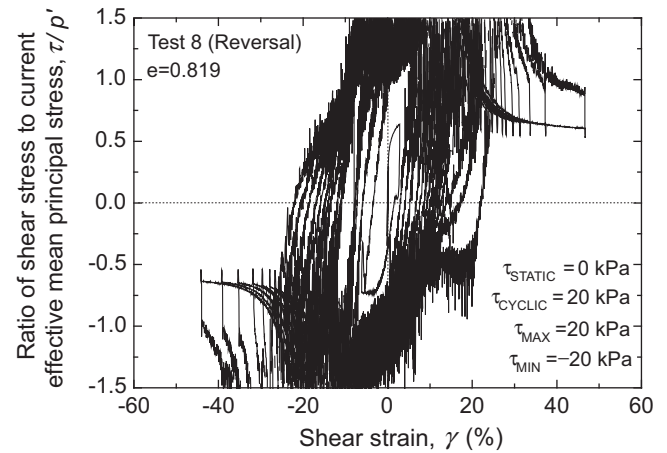

Fig. 12. Typical stress–strain relationship without correction for $\Delta \tau$ and $\Delta p'$.

should also be noted that, in the case of intermediate and non-reversal loadings, the $\Delta \tau$ values cannot be estimated due to the non-reversal stress conditions. Therefore, the $\Delta \tau$ values are always taken as zero (i.e., $\Delta \tau = 0$).

Figs. 12 and 13 show typical relationships between the shear stress ratio and the shear strain, without and with correction for the above $\Delta \tau$ and $\Delta p'$ values, respectively. In the case without correction for $\Delta \tau$ and $\Delta p'$ (i.e., $\Delta \tau = 0$, $\Delta p' = 0$) (Fig. 12), the shear stress ratio largely fluctuated and occasionally became extremely large due to division by zero (i.e., $p' = 0$ at the full liquefaction state). On the contrary, in the case with correction for $\Delta \tau$ and $\Delta p'$ (Fig. 13), such unstable behavior disappeared and the peak stress state (Peak State) was observed at a shear strain level (γ_{SA}^{peak}) of about $\pm 19\%$. The Peak State is followed by post-peak strain softening, as well as by State A. Therefore, the Peak State can be effectively considered as the state at which strain localization begins. On the other hand, State B seems to correspond to the end of strain-softening and the beginning of the residual stress state.
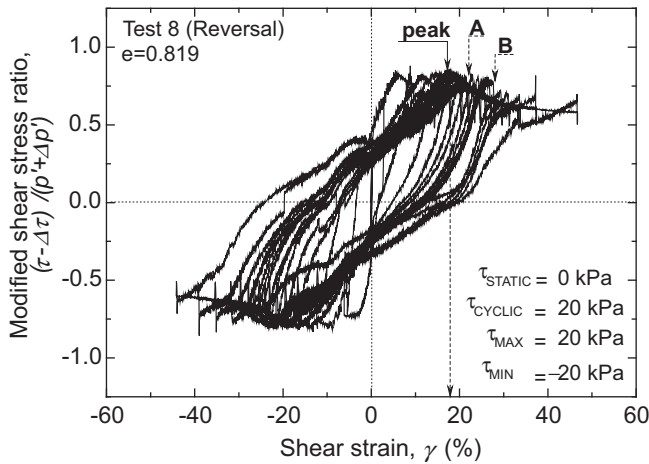

Fig. 10. Definition of $\Delta \tau$ and $\Delta p'$ based on effective stress path.

Fig. 13. Typical modified stress–strain relationship (i.e., after correcting for $\Delta\tau$ and $\Delta p'$) for reversal loading tests.
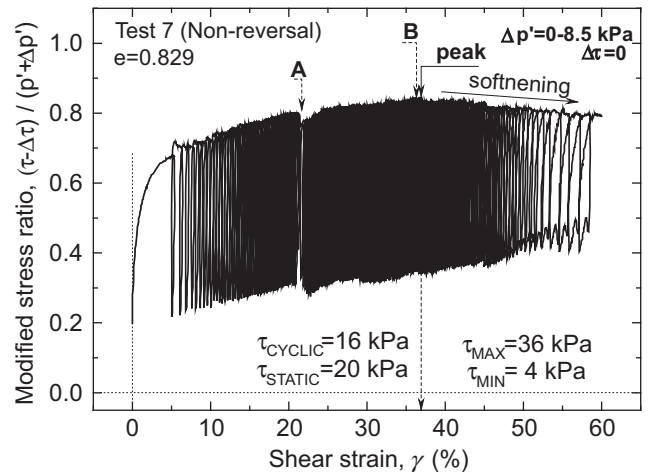

Fig. 15. Typical modified stress–strain relationship for non-reversal loading tests (c.f.4).
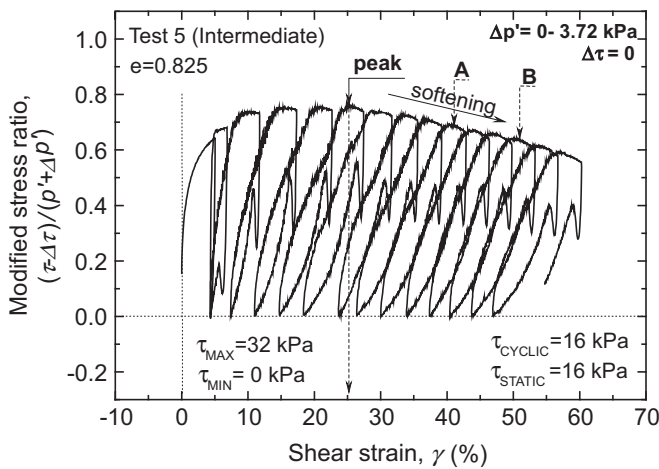

Fig. 14. Typical modified stress–strain relationship for intermediate tests (c.f. 3).
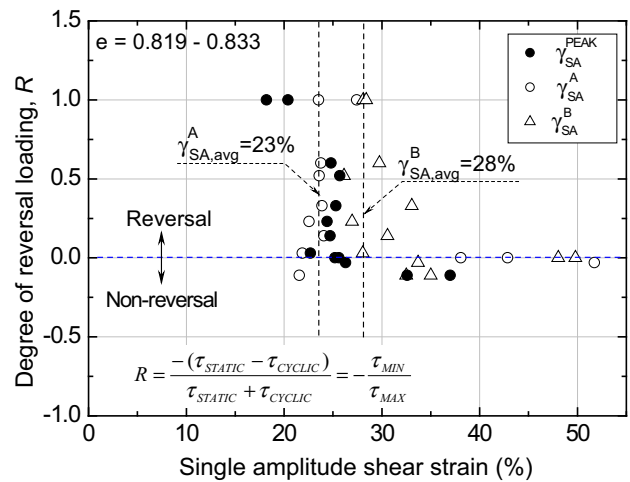

Fig. 16. Changes in strain-softening behavior in terms of γ_{SA}^{peak} and its comparison with γ_{SA}^{A} and γ_{SA}^{B}.

The test results reported in Fig. 14 show the case of intermediate loading. A clear stress peak followed by post-peak strain softening can be observed. In addition, as in the case of the reversal loading tests, the Peak State is followed by State A. Therefore, it can be regarded as the state at which strain localization begins.

Fig. 15 shows the test results of non-reversal loading. In this case, the stress peak is followed by strain-softening behavior. It should be noted that, contrarily to the cases of reversal and intermediate loading, State A preceded the Peak State, the reason(s) for which the authors cannot explain.

Fig. 16 compares the limiting strain values to the initial strain localization measured on the basis of the strain-softening properties of sand (i.e., γ_{SA}^{peak}) and the values for γ_{SA}^{A} and γ_{SA}^{B} presented previously.

The latter employed methodology, which utilizes non-constant $\Delta\tau$ and $\Delta p'$ values, first confirmed the γ_{SA} values to initiate strain localization by looking at changes in the q response (i.e., State A) and in the strain accumulation

properties (i.e., State B) in the case of stress reversal loading. Secondly, it provided reasonable limiting strain values in the case of intermediate loading tests that could not be properly defined by the previously employed methods. Although there are still uncertainties about the best method for evaluating strain localization limits in non-reversal loading tests, the above method suggests that limiting strain values for initiating strain localization are different between specimens showing liquefaction behavior (i.e., reversal and intermediate tests) and those that fail due to large deformation (i.e., non-reversal loading tests).

3.3. Comparison with observations of strain localization in previous studies

In the preceding study, Kiyota et al. (2008, 2010) investigated in detail where the strain localization occurs in liquefied soils by conducting cyclic undrained torsional shear tests without initial shear stress. In particular, on the
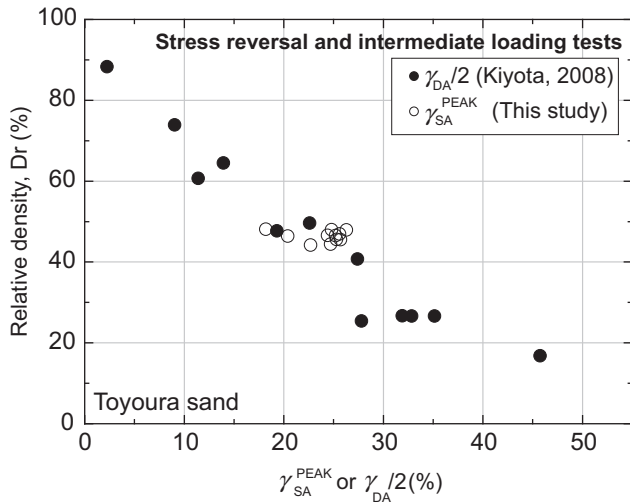
Fig. 17. Comparison between γ_{SA}^{peak} obtained in this study for stress reversal and intermediate loading tests and $\gamma_{DA}/2$ obtained by Kiyota et al. (2008).

basis of the undrained cyclic torsional shear test results, they reported the relationship between the limiting values of γ_{DA} and the relative density (Dr).

It should be noted that the values for $\gamma_{DA}/2$, evaluated by Kiyota et al. (2008, 2010), refer to the case of full stress reversal tests (i.e., no τ_{static} was applied); hence, they correspond well to the γ_{SA} values. Therefore, in Fig. 17, the limiting values for γ_{SA}^{peak} measured in this study for the case of reversal loading tests are compared with the limiting values for $\gamma_{DA}/2$ observed by Kiyota et al. (2008, 2010). It can be seen that the limiting value to initiate strain localization found in this study is consistent with the one reported by Kiyota et al. (2008, 2010).

This comparison, together with the one shown in Fig. 16, clearly shows that for saturated sand specimens showing liquefaction behavior (i.e., stress reversal and intermediate tests), the limiting value to initiate strain localization is independent of the cyclic stress amplitude and the applied initial static shear, but it may vary according to the density of the sand.

4. Summary and conclusions

The aim of this paper was to examine the effects of τ_{static} on the limiting value of shear strain at which strain localization appears during undrained cyclic torsional shear tests.

A series of undrained cyclic torsional shear tests, carried out on saturated loose Toyoura sand specimens up to a γ_{SA} exceeding 50%, was analyzed and non-uniform specimen deformation could be observed at strain levels higher than 20%. However, the initiation of strain localization could not be defined on the basis of visual observations. Therefore, the limiting values for $\gamma_{DA}/2$ and γ_{SA} shear strain were evaluated from the test results by looking at changes in the deviator stress response and strain accumulation properties.

In the case of the stress reversal loading tests, it was found that the greater the static shear level, the lower the $\gamma_{DA}/2$. On the other hand, γ_{SA} was rather constant with an increasing static shear stress level. These features suggest that to define the limiting value of strain required to initiate the strain localization of sand specimens subjected to initial static shear, γ_{SA} is a much more appropriate parameter than $\gamma_{DA}/2$, which was employed in previous studies.

However, in the case of the intermediate and the non-reversal loading tests, changes in neither the deviator stress response nor the strain accumulation properties could be properly used to evaluate the limiting strain values of γ_{SA}. Therefore, a different methodology, based on an evaluation of the strain-softening properties of sand was adopted.

In conclusion, under the test conditions employed for the current study, for loose sand specimens ($Dr = 44$–48%) showing liquefaction behavior (i.e., stress reversal and intermediate tests), the limiting strain value measured in terms of γ_{SA} was evaluated to be in the range of 23–28%, independent of the cyclic stress amplitude and the applied initial static shear.

Alternatively, in the case of the non-reversal loading tests, where liquefaction did not occur, the limiting strain value could not be properly defined, although various methods were employed.

Acknowledgments

Appendix A. Correction of deviator stress for membrane force

In performing torsional shear tests on a hollow cylindrical specimen, due to the presence of inner and outer membranes, the effect of the membrane force on the shear stress could not be ignored (Koseki et al., 2007; among others). In addition, the effect became significantly important when the shear strain reached extremely high levels (Kiyota et al., 2008; Chiaro et al., 2012).

In order to experimentally calibrate the membrane force developing at large strain levels, to be used to correct the measured shear stress, Chiaro et al. (2012) performed special tests consisting of cyclically shearing a water specimen under undrained conditions. Since the water specimen was sheared while preventing any vertical displacement of the top cap, the apparent deviator shear stress (q_m) induced by the extension of the membranes was observed. In Fig. 18, the measured relationship between the apparent deviator shear stress (q_m) and the shear strain
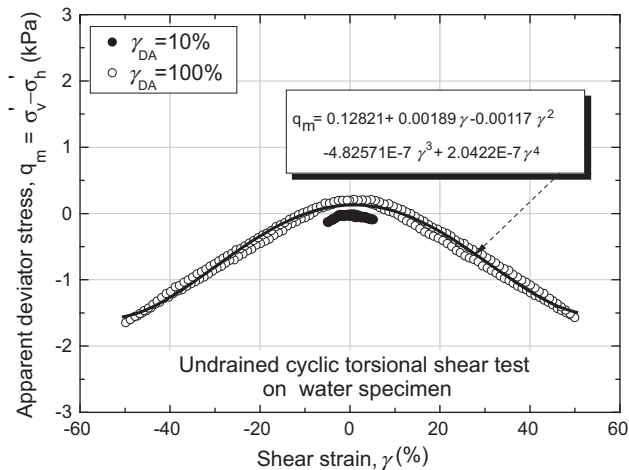
Fig. 18. Apparent deviator stress during undrained cyclic torsional shear loading on water specimen.

(γ) for the cycles of loading with $\gamma_{DA}=10\%$ and the one with $\gamma_{DA}=100\%$ are compared.

It should be noted that, in Fig. 5, the q values were corrected for the effect of the membrane force by employing the polynomial equation shown in Fig. 18. It can be seen that the membrane force does not have any significant effect on the limiting value of γ_{SA} or γ_{DA} to initiate strain localization in the specimen measured at State A at which the q value suddenly decreases.

References

Alshibli, K.A., Bastie, S., Sture, S., 2003. Strain localization in sand: plane strain versus triaxial compression. Journal of Geotechnical and Geoenvironmental Engineering, ASCE 129 (6), 483–494.

Alshibli, K.A., Sture, S., 2000. Shear band formation in plane strain experiments of sand. Journal of Geotechnical and Geoenvironmental Engineering, ASCE 126 (6), 495–503.

Chiaro, G., 2010 Deformation properties of sand with initial static shear in undrained torsional shear tests and their modeling, PhD thesis, Dept. of Civil Engineering, University of Tokyo, Japan.

Chiaro, G., Koseki, J., Sato, T., 2012. Effects of initial static shear on liquefaction and large deformation properties of loose saturated Toyoura sand in undrained cyclic torsional shear tests. Soils and Foundations 52 (3), 498–510.

Desrues, J., Chambon, R., Mokni, M., Mazerolle, F., 1996. Void ratio evolution inside shear bands in triaxial sand specimens studied by computed tomography. Geotechnique 46 (3), 529–546.

Finno, R., Harris, W., Mooney, M., Viggiani, G., 1996. Strain localization and undrained steady state of sand. Journal of Geotechnical Engineering, ASCE 122 (6), 462–473.

Finno, R., Harris, W., Mooney, M., Viggiani, G., 1997. Shear bands in plane strain compression of loose sand. Geotechnique 47 (1), 149–165.

Hamada, M., O'Rourke, T.D., Yoshida, N., 1994. Liquefaction-induced large ground displacement. Performance of Ground and Soil Structures during Earthquakes, 13th ICSMFE, 93–108.

Hamada, M., Yasuda, S. and Wakamatsu, K., 1988 Case studies on liquefaction-induced permanent ground displacement. In: Proceedings of 1st Japan–US Workshop on Liquefaction, Large Ground Deformation and their Effects on Lifeline Facilities, pp. 3–21.

Ishihara, K., Yasuda, S. and Nagase, H., 1996 Soil Characteristics and ground damage, Soils and Foundations, Special Issue on Geotechnical Aspects of the January 17 1995 Hyogoken–Nambu Earthquake, pp. 109–118.

Jang, D.J., Frost, J.D., 2000. Use of image analysis to study the microstructure of a failed sand specimen. Canadian Geotechnical Journal 37 (5), 1141–1149.

Kiyota, T., Sato, T., Koseki, J., Mohammad, A., 2008. Behavior of liquefied sands under extremely large strain levels in cyclic torsional shear tests. Soils and Foundations 48 (5), 727–739.

Kiyota, T., Koseki, J., Sato, T., 2010. Comparison of liquefaction-induced ground deformation between results from undrained cyclic torsional shear tests and observations from previous model tests and case studies. Soils and Foundations 50 (3), 421–429.

Kokusho, T., 1999. Formation of water film in liquefied sand and its effects on lateral spread. Journal of Geotechnical and Geoenvironmental Engineering, ASCE 125 (10), 817–826.

Kokusho, T., 2000. Mechanism of water film generation and lateral flow in liquefied sand layer. Soils and Foundations 40 (5), 99–111.

Koseki, J., Kiyota, T., Sato, T. and Mohammad, A.M., 2007 Undrained cyclic torsional shear tests on sand up to extremely large strain levels. In: Proceedings of International Workshop on Earthquake Hazard and Mitigation, Guwahati, India, pp. 257–263.

Koseki, J., Yoshida, T., Sato, T., 2005. Liquefaction properties of Toyoura sand in cyclic torsional shear tests under low confining stress. Soils and Foundations 45 (5), 103–113.

Lade P.V., 1982 Localization effects in triaxial tests on sand. In: Proceedings of Conference on Deformation and Failure of Granular Media, Balkema, Rotterdam, pp. 461–471.

Peters, J.F., Lade, P.V. and Bro, A., 1988 Shear band formation in triaxial and plain strain tests, In: Proceedings of Advances in Triaxial Testing of Soil and Rock, STP 977, ASTM, Philadelphia, PA, pp. 604–627.

Sadrekarimi, A., Olson, S.M., 2009. A new ring device to measure the large displacement shearing behavior of sand. Geotechnical Testing Journal, ASTM 32 (3), 1–12.

Sadrekarimi, A., Olson, S.M., 2010. Shear band formation observed in ring shear tests on sandy soils. Journal of Geotechnical and Geoenvironmental Engineering, ASCE 136 (2), 366–372.

Tatsuoka, F., Nakamura, S., Huang, C.C., Tani, K., 1990. Strength anisotropy and shear band direction in plane strain tests of sand. Soils and Foundations 30 (1), 35–54.

Tatsuoka, F., Sonoda, S., Hara, K., Fukushima, S., Pradhan, T.B.S., 1986. Failure and deformation of sand in torsional shear. Soils and Foundations 26 (4), 79–97.

Towhata, I. and Gallage, C.P.K. (1993): Rate-dependency of sand under low effective stress as observed in laboratory shear tests. In: Proceedings of 8th U.S.–Japan Workshop on Earthquake Resistance Design of Lifeline Facilities and Countermeasures Against Liquefaction, Tokyo, Japan, paper II-7, pp. 473–448.

Viggiani, G., Kuentz, M., Desrues, J., 2001. An experimental investigation of relationship between grain size and distribution and shear banding in sand. In: Vermeer, S. (Ed.), Continuous and Discontinuous Modelling of Cohesive–Frictional Material. Springer, New York, pp. 111–126.

Wahyudi, S., Miyashita, Y. and Koseki, J. (2012): Observation of shear banding behavior of sand in torsional shear test using image analysis technique, Advances in Multiphysical Testing of Soils and Shales, Springer, 201–206.

Yasuda, S., Nagase, H., Kiku, H., Uchida, Y., 1992. The mechanism and a simplified procedure for the analysis of permanent ground displacement due to liquefaction. Soils and Foundations 32 (1), 149–160.

Yoshimi, Y., Oh-oka, H., 1975. Influence of degree of shear stress reversal on the liquefaction potential of saturated sand. Soils and Foundations 15 (3), 27–40.